Low-Reynolds-Number Airfoil Design for the M.I.T. Daedalus Prototype: A Case Study

Mark Drela*
Massachusetts Institute of Technology, Cambridge, Massachusetts

The rationale used for the aerodynamic wing design of the prototype long-range human-powered aircraft Light Eagle is presented. Three different airfoils, designed for chord Reynolds numbers of 500,000,375,000, and 250,000 were used across the wingspan. The airfoil design rationale centered on minimizing the losses in the transitional separation bubbles typically occurring on airfoils at Reynolds numbers of less than 1 million. Structural and manufacturing constraints were also a consideration in the airfoil design, although to a lesser extent. Airfoil performance prediction during the design process was done entirely through numerical simulation. The numerical model employs the Euler equations to represent the inviscid flow, and an integral boundary-layer formulation to represent the viscous flow. Strong viscous-inviscid coupling and an amplification transition criterion included in the overall equation system permit calculation of transitional separation bubbles and their associated losses. Flow visualization tests performed on the Light Eagle at various lift coefficients in towed flight revealed transition occumng very near the intended position on the wing surface except within a few chords of the tip, where the flow appeared to be turbulent over most of the upper surface. Total drag aircraft polars obtained from the measured aircraft energy time history in glide contained too much scatter to be used as quantitative test data but did reproduce the basic trends of the calculations, including maximum lift coefficient levels.

Nomenclature

b =wingspan
c =airfoil chord
C_D =profile drag coefficient, aircraft drag coefficient
C_L =profile lift coefficient, aircraft lift coefficient
C_M =profile pitching moment coefficient
C_f =skin friction coefficient $= \dfrac{2\tau_{\text{wall}}}{\rho u_e^2}$
C_p =pressure coefficient $= \dfrac{2(p-p_\infty)}{\rho u_\infty^2}$
H =shape parameter $= \dfrac{\delta^*}{\theta}$
$\tilde{n}$ =exponent of most-amplified Tollmien-Schlichting wave amplitude
Re =chord Reynolds number $= \dfrac{\rho u_\infty c}{\mu}$
Re_θ =momentum thickness Reynolds number $= \dfrac{\rho u_e \theta}{\mu}$
u_e =boundary-layer (BE) edge velocity
u_{inv} =inviscid airfoil surface velocity (BL absent)
x,y =chordwise, spanwise coordinates
α =airfoil angle of attack
δ^* =displacement thickness $= \int \left(1-\dfrac{u}{u_e}\right) d\eta$
θ =momentum thickness $= \int \dfrac{u}{u_e}\left(1-\dfrac{u}{u_e}\right) d\eta$
ρ =air density
μ =air viscosity
τ =shear stress
ξ,η =boundary layer coordinates

Received Sept. 11, 1987; revision received Dec. 22, 1987.

*Assistant Professor, Department of Aeronautics and Astronautics. Member AIAA.

I. Introduction

THE Light Eagle human-powered aircraft (HPA) shown in Fig. 1 currently holds the Federation Aeronautique Internationale (FAI) closed-course world distance record of 36.4 miles, established in 2 h 14 min on January 23, 1987. The Light Eagle was constructed in 1986 to serve as a prototype for the Daedalus aircraft, intended to recreate in 1988 the mythical flight of Daedalus from Crete to the mainland of Greece. The 69 mile over water distance and the rather high flight speed of 15 mph (constrained by the short duration of calm weather periods in the Aegean Sea) place extreme demands on the structural efficiency and the aerodynamic performance of the prototype aircraft. The long-duration power level available from a good athlete (about 3 W per k of body weight) dictated an overall aircraft lift-to-drag ratio of 40:1 or better. This precluded the use of extensive external wire bracing common on low-power human-powered aircraft. Only a single lift wire was used as a concession to structural efficiency.

The extreme aspect ratio of the Light Eagle wing (39.4: 1 in the final version), minimal fuselage pod and tail surfaces, and the lack of extensive external wire bracing, resulted in the wing profile drag contribution being 40% of the total drag. This placed high demands on the performance of the wing airfoil, the design of which was complicated by a myriad of structural and manufacturing constraints.

Airfoil flows on HPA's are well into the so-called low-Reynolds-number regime (less than 1 million), where airfoil performance is strongly influenced by transitional separation bubbles. These provide a mechanism for rapid transition at the beginning of an airfoil's pressure recovery region. If the bubble is kept small, its mixing losses can be kept down to reasonably low values, often less than those resulting from a mechanical transiton device. The bubble also moves with angle of attack, giving a wider low-drag range than would be possible with a fixed transition strip. On the negative side, the losses in a relatively large bubble can result in dramatic airfoil drag increases. For these reasons, the control of transitional separation bubble position and size is one of the most important considerations in low-Reynolds-number airfoil design.

Separation bubble control on the Light Eagle airfoils was sought only via the surface-pressure distribution. Often, various artificial transition-inducing devices (roughness,

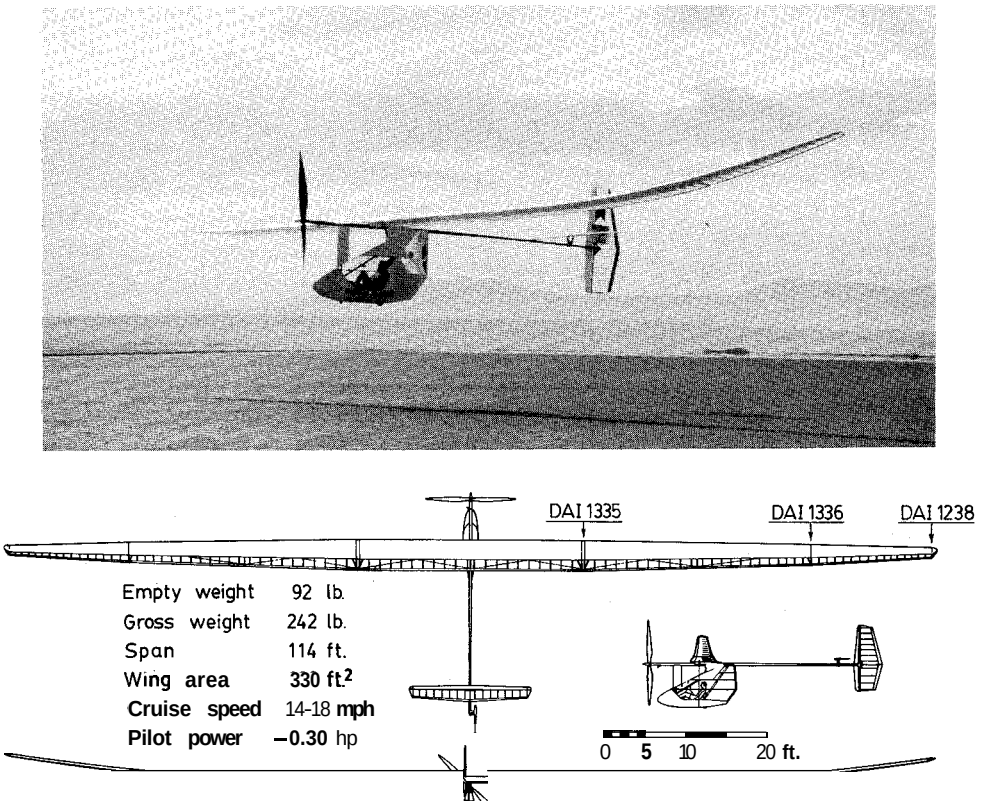

Fig. 1 The Light Eagle human-powered aircraft.

strips, blowing, etc.) can also be used, and have shown to improve airfoil performance under certain conditions, especially at Reynolds numbers below 200,000.[1-3] These were not considered for the Light Eagle airfoils since transition devices are rather impractical on any HPA wing that depends on extensive laminar flow. Just before a flight (typically at dawn when winds are most calm), such a wing must be rapidly wiped clean of continuously accumulating dew or frost, and protruding transition devices mounted on the delicate styrofoam/Mylar surface could not withstand such treatment. Such a surface also does not lend itself well to installation of a pneumatic turbulator system. Furthermore, the operating C_L range of HPA's is quite narrow (between -1.0 and 1.4 for the Light Eagle), so that fairly precise bubble control is possible with pressure distribution alone.

Besides bubble losses, other aerodynamic considerations such as maximum lift coefficient and pitching moment enter the airfoil design picture. This paper presents the various design issues which arise in low-Reynolds-number airfoil design, stressing the tradeoffs that occur between the various structural, aerodynamic, and manufacturing requirements. Samples will be drawn from the particular design of the Light Eagle wing airfoils.

II. Components of Profile Drag

Airfoil design is strongly driven by the minimization of profile drag, which has two components: friction drag and form drag. Friction drag is a direct result of viscous shear forces tangential to the surface. Form drag is caused by the displacement effects of the boundary layers and wake modifying the inviscid surface velocity, creating a net aft component of the pressure forces normal to the airfoil surface. At Reynolds numbers below 1 million or so, a transitional separation bubble, (Fig. 2), contributes significantly to the form drag via the lower pressure over the bubble acting over the aft-facing airfoil surface. At Reynolds numbers below 150,000, this bubble drag (or "bubble loss") often dominates the total drag.

It is useful to express profile drag in terms of boundary layer momentum losses. Profile drag is equal to the total

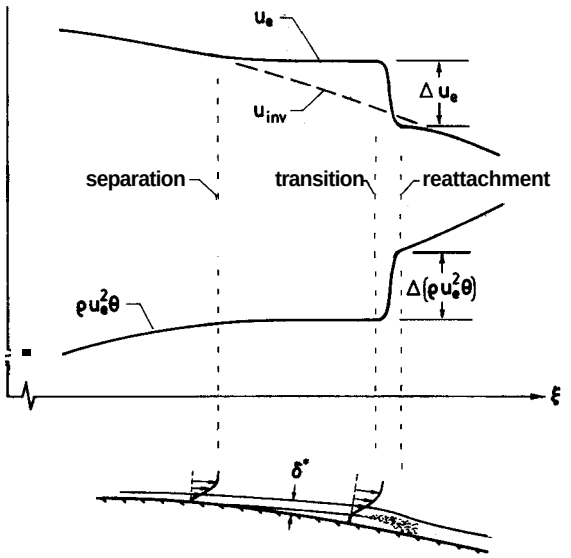

Fig. 2 Edge velocity and momentum deficit jumps at reattachment.

momentum defect $\rho u_e^2\theta$ in the wake far behind the airfoil. The streamwise development of $\rho u_e^2\theta$ in the boundary layers and wake is governed by the von Kármán integral momentum equation:

$$\frac{1}{\rho u_e^2\theta}\frac{\mathrm{d}(\rho u_e^2\theta)}{\mathrm{d}\xi} = \frac{C_f}{2\theta} - \frac{H}{u_e}\frac{\mathrm{d}u_e}{\mathrm{d}\xi} \tag{1}$$

The edge velocity gradient has the shape parameter H as a coefficient, implying that pressure recovery in separated regions, such as at the end of a bubble, is detrimental to achieving low drag. In fact, the edge velocity and momentum defect gradients at the transition-reattachment region are so

steep, that one can consider the changes in u_e and $\rho u_e^2\theta$ over this region as discontinuous jumps. Neglecting the skin friction term which is small in separation bubbles, the von Kármán Eq. (1) can be integrated over the transition-reattachment region to give a relation between the fractional u_e and $\rho u_e^2\theta$ jumps.

$$\frac{\Delta(\rho u_e^2\theta)}{\rho u_e^2\theta} \simeq -H\frac{\Delta u_e}{u_e} \tag{2}$$

where $\rho u_e^2\theta$, H, and u_e can be considered as average quantities over the region.

Equation (2) can also be rewritten in terms of the absolute jumps in u_e and $\rho u_e^2\theta$:

$$\Delta(\rho u_e^2\theta) = -\rho u_e \delta^* \Delta u_e \tag{3}$$

The direct drag increment $\Delta(\rho u_e^2\theta)$ due to turbulent reattachment is thus proportional to the average mass defect $\rho u_e\delta^*$ and the edge velocity jump Δu_e over the high-gradient region. To keep this loss small, the mass defect $\rho u_e\delta^*$ at transition must be kept small. Equivalently stated, the distance of the free shear layer from the wall must not be excessive at transition, since the stagnant fluid under the shear layer must mix out for reattachment to occur. This turbulent mixing is the physical mechanism through which the additional work done on the airstream by the airfoil via the bubble pressure drag is dissipated into heat. The actual drag increase on the whole airfoil will likely be greater than the bubble momentum deficit jump, since the latter is invariably "amplified" by the airfoil's pressure recovery region.

One way to decrease the overall momentum defect rise over the bubble and hence lessen airfoil drag is to shorten it by forcing transition farther upstream. However, it is also undesirable to eliminate the bubble completely since this will increase turbulent skin fraction drag as shown in Fig. 3. Clearly, an optimum transition location exists, usually close to the laminar separation point. It is also obvious that this optimum location will move with angle of attack. The challenge in low-drag airfoil design is to achieve transition at or near this point over as much of the operating range of the airfoil as possible. At low Reynolds numbers, transition generally occurs past the separation point, so control of bubble losses rather than minimizing turublent skin friction is the primary concern.

III. Viscous-Inviscid Interaction

Transitional separation bubbles cannot be adequately described by the boundary layer equations alone, since it is the potential flow which sets the distance of a separated shear layer from the wall (approximately equal to δ^*), and not the boundary layer equations. The latter merely enforce u_e to be nearly constant (they describe the strong reaction of the stagnant viscous fluid under the shear layer to alleviate any imposed pressure gradients). This is a complete role reversal from the case of attached flow assumed by classical boundary layer theory, where the potential flow determines u_e and the vixcous flow subsequently determines 6*.

For prediction of airfoil flows with separation bubbles, it is clearly necessary to allow the viscous layer to influence the potential flow. To first order, this can be done by invoking either the displacement surface or the wall transpiration concepts of Lighthill.[4] In the ISES code (described later) used to design the Light Eagle airfoils, the displacement thickness concept is used to modify the airfoil contour seen by the inviscid flow. For the purpose of understanding how bubble losses are influenced by the potential flow, it is more convenient to use the wall transpiration model, where the viscous layer is replaced by a distribution of sources along the wall. Superposition of the velocity field of these sources gives the change between the actual $(u,)$ and the inviscid (u_{inv}) velocities in terms of an integral over the entire displacement thickness distribution. For a flat wall, this expression is

$$\Delta u_{\text{inv}}(\xi) \equiv u_e(\xi) - u_{\text{inv}}(\xi) = \frac{1}{\pi}\int \frac{\mathrm{d}(u_e\delta^*)}{\mathrm{d}s}\frac{\mathrm{d}s}{\xi - s} \tag{4}$$

Note that the edge velocity jump Δu, over the transition-reattachment region is approximately equal to Δu_{inv} there, as suggested by Fig. 2. Also, it is clear from Fig. 2 that for a given bubble length, the transition-reattachment jump Δu, will be proportional to the inviscid velocity gradient $\mathrm{d}u_{\text{inv}}/\mathrm{d}\xi$. Furthermore, because the δ^* distribution in the bubble itself produces the dominant contribution to the integral in Eq. (4), it follows that δ^* at some given distance downstream of the separation point will be roughly proportional to $\mathrm{d}u_{\text{inv}}/\mathrm{d}\xi$ as well. The net result is that Δu_e and δ^* at reattachment both increase with increasing inviscid pressure gradient over the bubble, making the bubble losses very strongly dependent on this inviscid pressure gradient.

IV. Separation Bubble Control

In airfoil flows, natural transition is initiated by unstable Tollmien-Schlichting waves reaching a critical amplitude. Provided the Reynolds number if high enough for instability to exist, the growth rate of the most-amplified wave is very strongly dependent on the local shape parameter (Fig. 4) and is inversely proportional to the local momentum thickness 8 and hence $\sqrt{Re}$. At low Reynolds numbers, a high shape parameter corresponding to separated flow is usually needed to achieve transition within the airfoil chord length and prevent massive separation. In practice, it is possible to achieve sufficiently early transition with a more careful aerodynamic design of the overall inviscid pressure distribution (as discussed earlier, artificial transition devices were not considered for the Light Eagle airfoils). The goal is obtaining transition before the separated shear layer moves too far from the airfoil surface.

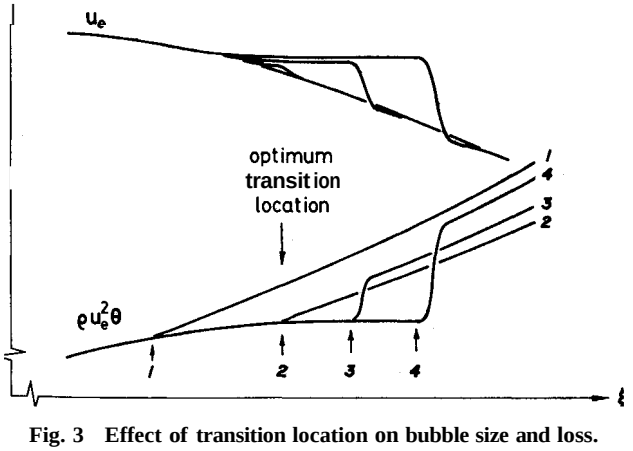

Fig. 3 Effect of transition location on bubble size and loss.

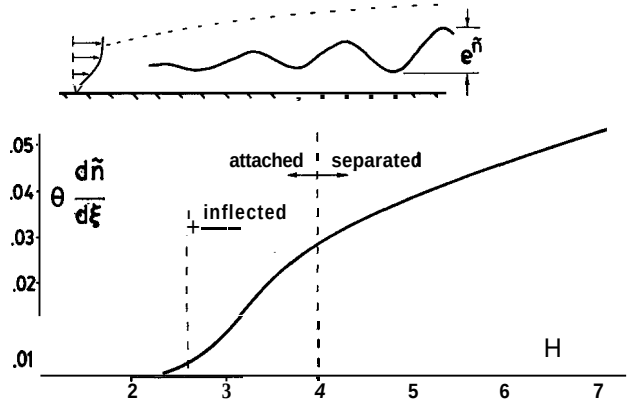

Fig. 4 Growth rate of most-amplified Tollmien-Schlichting disturbance.

As pointed out by Wortmann,[5] an effective technique of obtaining good overall amplification at low Reynolds numbers is to destabilize the boundary layer near the leading edge of the airfoil. By applying a long weak adverse pressure gradient over the laminar "transition ramp," the boundary layer profiles can be made to be inflected and favor instability growth while still remaining attached. Ideally, the laminar profiles should be held at the constant shape parameter H which will cause transition to occur just at the start of the steep turbulent pressure recovery region with no separation. If the airfoil were to operate at one C_L value and one Reynolds number, its ideal pressure distribution would have the shape shown in Fig. 5 along with a modified distribution and their associated polars. In practice, the ideal pressure distribution will have disasterous off-design performance, since the laminar boundary layer over the ramp must be held quite close to separation, and hence will be very sensitive to α variation. Only a small α increase is needed to substantially increase H near the leading edge, which causes the transition point to run forward quickly with severe consequences for lift and drag. Conversely, a decrease in α causes the transition point to extend into the steep turbulent recovery region, rapidly increasing the bubble losses. Such a one-point airfoil will also be very sensitive to unexpected surface waviness or roughness, either of which may cause premature transition.

The modified pressure distribution shown in Fig. 5 has its transition ramp arched and gradually steepened into the turbulent recovery region. The shape parameter now gradually increases downstream and a separation bubble results. Most of the amplification now occurs towards the back of the ramp and in the bubble, so that an α increase or surface imperfections will not cause transition to run forward rapidly. Although the modified airfoil has higher drag than the ideal airfoil at its design point, it is clearly superior in all other aspects.

The shape of the airfoil's transition ramp can be systematically altered to tailor the airfoil's off-design performance. Specifically, the length, slope, and arch of the transition ramp can be varied to control bubble motion and bubble losses over the airfoil's operating range. Other airfoil parameters such as C_M and $C_{L\max}$ are also favorably or adversely affected, and these factors, discussed in more detail in the following section, must be considered in the design of the airfoil.

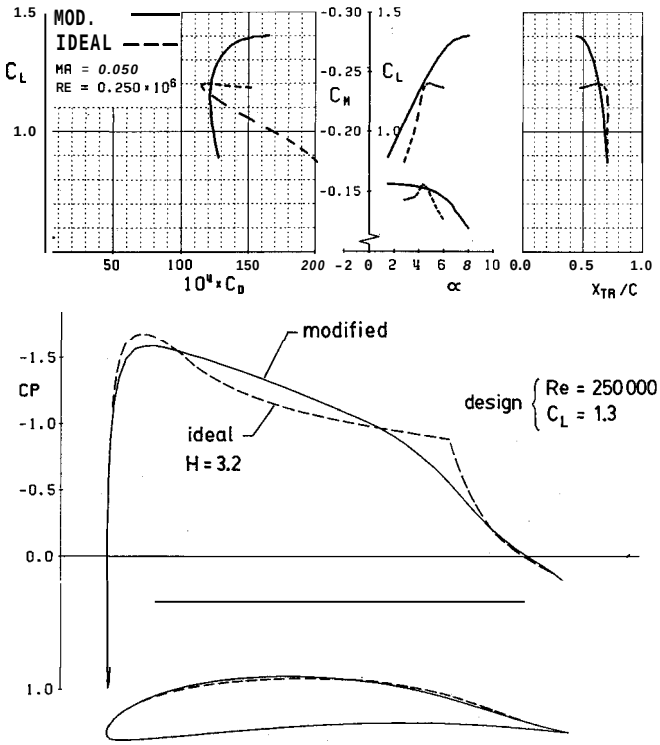

Fig. 5 Ideal and modified design pressure distributions and resulting calculated polars.

V. Airfoil Design Parameters

The airfoil design process is usually aimed at obtaining the airfoil that maximizes the overall performance of the aircraft. Invariably, the airfoil design is influenced by a myriad of constraints and requirements that usually conflict. In principle, the design problem can be formally expressed as a constrained maximization (or optimization) problem, with the variables being some set of airfoil design parameters (thickness, camber, etc.). The solution to such a problem is that a particular combination of design parameters that maximizes some measure of performance such as aircraft L/D, becomes subject to a number of constraints such as structural integrity, tolerance of surface debris, ease of manufacture, etc. Some algorithm (such as an aerodynamic code) that takes in the design parameters and outputs performance is, of course, required. This approach to airfoil design has a strong mathematical appeal, but usually turns out to be nearly useless in practice. The biggest problem is that important constraints are often impossible to quantify in a reliable manner, either by nature (e.g., ease of manufacture), or by lack of sufficiently accurate data (e.g., tolerance to surface debris). A lesser but still nontrivial problem is the formulation of an adequate set of design parameters. The most general set would be the 100 or so x-y coordinate pairs describing the airfoil shape, but the resulting optimization problem would be prohibitively expensive to solve.

The most effective airfoil design process appears to be one where a knowledgable and experienced designer makes objective (and sometime subjective) decisions about the relative merits of conflicting design parameters. Ideally, such decisions are based on all available data (including calculation results). More often that not, accurate data is scarce, and the designer must rely on sheer intuition.

The good designer also uses a smaller and more appropriate set of design parameters than all the coordinate values defining the airfoil. A much better choice is to use a smaller set of smooth geometric modes, such as thickness front camber, aft camber, leading edge radius, trailing edge angle, etc., especially in the early design stages when the design is being "roughed out." In addition to these geometric design parameters, the aerodynamic parameters are also important, as they are the characteristics of the airfoil surface pressure distribution. Their advantage is that they have a much more direct bearing on the airfoil performance than the geometric parameters.

A. Aerodynamic Parameters

For low-Reynolds-number airfoils, the dominant aerodynamic parameters are the length, average slope, and arch of the suction side transition ramp as mentioned in the previous section. Figures 6 and 7 show the effects these ramp characteristics have on the drag polar of a "base" airfoil. Clearly, each characteristic has both favorable and detrimental effects on the airfoil performance. Bubble loss is reduced by a long, relatively steep transition ramp with minimal arch, all of which enhance Tollmien-Schlichting disturbance growth. A long ramp will result in more laminar flow and will thus give a reduction in the skin friction drag as well. An arched transition ramp has a wider useable angle-of-attack range and produces more resistance to surface imperfections than a concave ramp but has larger bubble losses hence and more drag on-design. An arched ramp also favors a high $C_{L\max}$ because it delays the leading edge pressure spike as α is increased. Ramp slope and length also affect $C_{L\max}$, but to a lesser degree. The ramp variation comparisons in Figs. 6 and 7 were performed at $Re = 250{,}000$. In general, lower Reynolds numbers will increase the relative effects of ramp variation and vice versa.

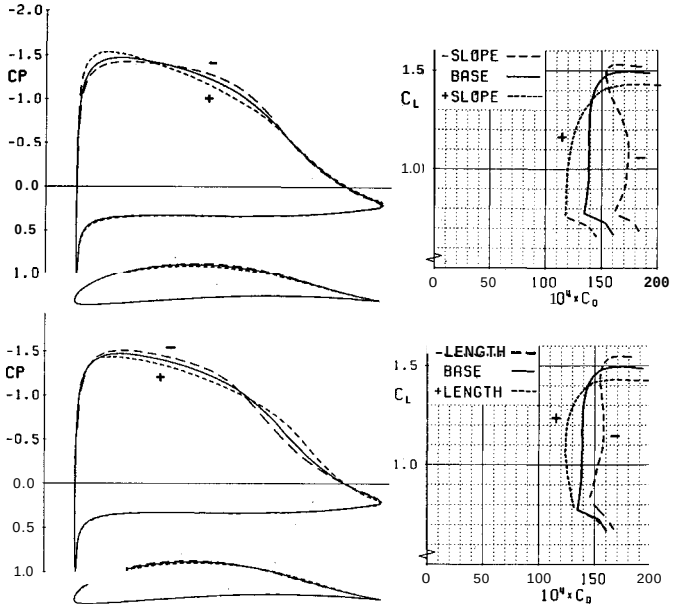

Fig. 6 Effect of transition ramp slope and length on performance: design $C_L = 1.2$, $Re = 250{,}000$.

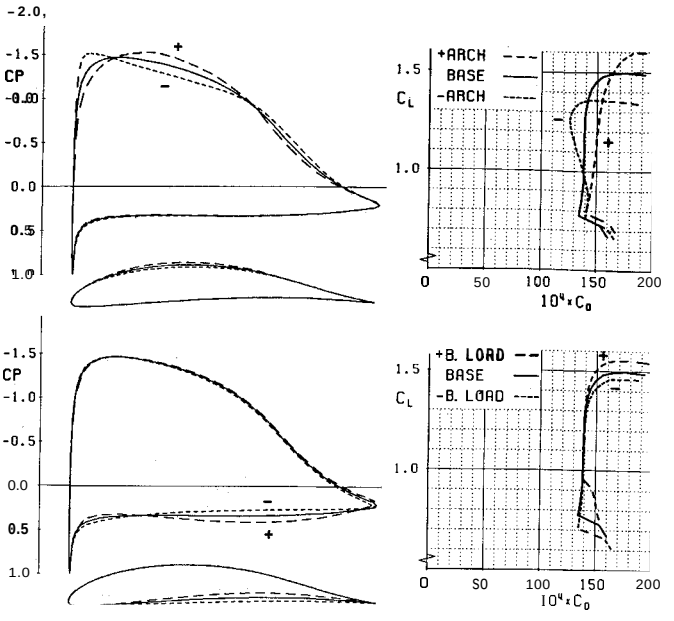

Fig. 7 Effect of transition ramp arch (design $C_L = 1.2$) and bottom loading (upper $C_p \simeq$ const) on performance: $Re = 250{,}000$.

Table 1 Effects of aerodynamic design parameters

Increasing	Increases	Decreases
Ramp length	C_M	Bubble loss, friction drag, $C_{L\max}$
Ramp slope	Poor surface degradation	C_M, bubble loss, $C_{L\max}$
Ramp arch	Bubble loss, $C_{L\max}$, α range	Poor surface degradation
Bottom loading	C_M, $C_{L\max}$	Thickness, α range
Recovery concavity	$C_{L\max}$, bubble loss	Aft thickness, drag creep

Another significant aerodynamic parameter is the degree of bottom loading, illustrated in Fig. 7. A larger bottom loading invariably results in a larger $C_{L\max}$ and a large maximum L/D, but a smaller α range due to earlier transition on the lower surface as α is reduced. Also, increasing bottom loading will reduce the airfoil thickness and increase C_M, both of which are likely to increase the structural weight.

An aerodynamic parameter that deserves mention is the pressure distribution over the turbulent recovery region. The largest pressure rise over a given airfoil length will be obtained from a strongly concave Stratford-type distribution, giving high $C_{L\max}$ values and minimal drag rise as stall is approached. However, such a distribution with a steep initial slope is incompatible with maintaining a mild inviscid pressure gradient over the bubble, and will usually produce a nearly-cusped trailing edge. On the Light Eagle airfoils, moderation of the recovery concavity was necessary primarily to achieve a structurally feasible trailing edge angle.

The effects of the various aerodynamic parameters discussed above can be summarized in Table 1.

B. Geometric Parameters

Some of the more important geometric parameters are the maximum airfoil thickness, the trailing-edge angle, and the leading-edge radius. In principle these parameters are automatically determined if the surface pressure distributions are specified. In practice, it is more convenient and productive to specify these geometric parmeters directly rather than via the surface pressure distributions. As a result, some control over the surface pressures is lost, but this must be accepted as one of the tradeoffs that arise in airfoil design.

Maximum airfoil thickness is usually driven by a drag-stiffness and/or drag-weight tradeoff since the airfoil determines the maximum spar depth and the enclosed torsion area if a stressed-skin wing structure is used. In the Light Eagle wing, the spar consists of a relatively large diameter, thin-wall carbon fiber (CF) tube that carries all the wing torsion loads and provides separation for the small CFR spar cap tubes that carry the bending loads (see Fig. 8). The diameter of the large torsion tube was limited by minimum gage and shell buckling constraints, and not by the airfoil thickness. The Light Eagle wing thus represents one of those rare instances where airfoil thickness was solely determined by aerodynamic requirements (a wide drag bucket). Increasing airfoil thickness increases the drag bucket width simply because it increases the α variation needed to generate a leading-edge pressure spike on either surface.

The trailing-edge angle is usually driven by structural and manufacturing constraints, although aerodynamics enter the picture as well. The proverbial cusped trailing edge is compatible with a concave pressure recovery and has the least form drag, although at low Reynolds numbers the substantial displacement effects at the trailing edge tend to hide the effects of any local geometric details. In any case, the cusped trailing edge is quite impossible to construct. In practice, either the trailing edge angle is made finite, or the upper and lower surfaces are made parallel but separated by a finite base thickness. The design is often decided by the wing construction method to be used. In the case of the Light Eagle wing, the trailing-edge strip consists of an acrylic foam/carbon fiber/aramid fiber/epoxy sandwich. The sandwich is laid up flat and oven-cured under vacuum. This allows a perfectly sharp trailing edge and the rather small trailing-edge angle of 7 deg, but does not allow a curved camber line over the trailing edge strip (last 5% chord).

The effects of the leading-edge radius differ depending on what type of airfoil is under consideration. A small leading-edge radius generally delays the leading-edge pressure spike at

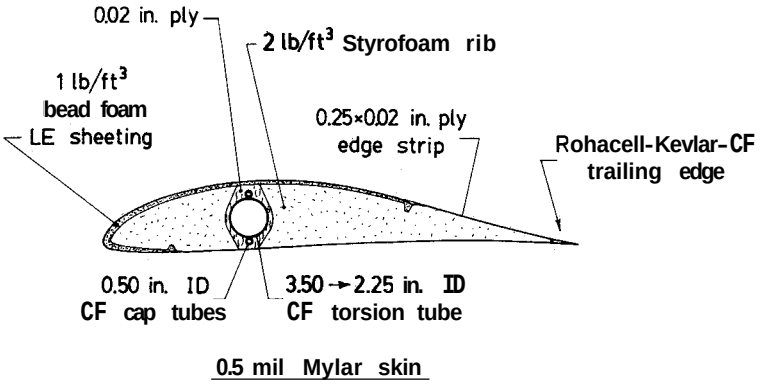

Fig. 8 Typical Light Eagle wing cross section.

Table 2 Effects of geometric design parameters

Increase in	Increases	Decreases
Thickness	Drag, α range,	Structual weight
Leading edge radius	Drag, imperfection tolerance	α range
Trailing edge angle	Foam drg	$C_{L\max}$

high angles of attack, but, once the spike appears, it is more intense than for a large leading-edge radius. The all-turbulent airfoils found on aluminum general-aviation aircraft typically stall long after the leading-edge spike appears. Hence, a larger leading-edge radius and the accompanying weaker pressure spike produces higher $C_{L\max}$ figures on such airfoils. In contrast, laminar airfoils typical of sailplanes and composite homebuilt aircraft stall shortly after a leading-edge spike occurs causing loss of laminar flow. On such airfoils, a small leading-edge radius leads to higher $C_{L\max}$ values. In general, the spike-delaying effect of a small leading-edge radius also gives a wider drag bucket than a large leading-edge radius in laminar flow airfoils. The alternative method of widening the drag bucket—by increasing the airfoil thickness—usually leads to higher overall drag values. Thus, for a given bucket width, the airfoil with a smaller leading-edge radius will have lower drag.

The primary problem with a small leading-edge radius is that it is more sensitive to inaccurate construction and surface debris. Since the Light Eagle leading edge is low-density polystyrene foam, which is difficult to shape very accurately, a leading edge radius of 1.25% chord (roughly double that of typical sailplane airfoils) was chosen for the Light Eagle airfoils. This concession to ease of manufacture and surface imperfection tolerance entailed a predicted profile drag penalty of about 3%.

The various effects of the geometric parameters discussed above are summarized in Table 2.

VI. Computational Airfoil Design

With the advent of computational airfoil analysis methods, the designer has a powerful tool for guiding the airfoil design process, since the influence of the many design parameters can be determined more easily and thoroughly than in a wind tunnel. Systematic modification of the airfoil geometry is also vastly more efficient when done by software instead of by hand.

A code that takes an airfoil geometry as input and calculates its performance is commonly referred to as a direct code. When aerodynamic design parameters are employed in the design process, it is necessary to have an inverse code that generates airfoil geometry from a specified pressure distribution. Inverse codes are often called design codes, which is inappropriate since the overall design process usually requires many more conventional direct calculations than inverse calculations. There are numerous incompressible and compressible algorithms that can perform the inverse calculation task.[6–8] It is never possible to specify a completely arbitrary surface pressure distribution and obtain a closed, physically realizable airfoil, since the specified pressure distribution must satisfy certain integral constraints as proved by Lighthill.[9] Hence, a good inverse code will take the liberty of modifying the specified surface pressures so that these constraints are satisfied. In practice, only minor modifications are required.

All of the performance prediction in the design process of the Light Eagle airfoils was performed by the direct/inverse ISES code.[8,10] It has been verified for a number of transonic and low-Reynolds-number airfoils.[11,12] ISES is a zonal method that employs the steady compressible Euler equations to describe the inviscid outer flow, and a two-equation lagged dissipation integral formulation to describe the boundary layers and wake. The effect of the viscous regions on the inviscid flow is modeled by the displacement surface concept. The overall discrete equation system is solved by a full Newton method. This solution technique performs stable calculation of flows with limited separation regions without elaborate viscous/inviscid iteration techniques.

The ISES code uses an e^9 type transition prediction method similar to that of Smith and Gamberoni,[13] which models the spatial growth rate of Tollmien-Schlichting waves which lead to transition. The growth rates are determined from solutions to the Orr-Sommerfeld equation correlated with the local shape prameter and momentum thickness. The first-order ODE, which describes the downstream growth of the most-amplified Tollmien-Schlichting disturbance, is discretized and included in the overall viscous-inviscid equation system. This approach appears to give reliable prediction of transition both in attached boundary layers and in separation bubbles.[11]

VII. Light Eagle Airfoils

The strongly tapered planform of the Light Eagle wing resulted in a substantial chord Reynolds number variation (540,000–180,000) across the span. In this range, a single airfoil typically experiences drastic changes in performance, which is mainly due to the variation in separation bubble size and losses. Three different airfoils (DAI 1135, DAI 1336, DAI 1238) optimized for three different Reynolds numbers (500,000, 375,000, 250,000) were therefore developed. The three airfoils were used at the planform breaks of the Light Eagle wing as shown in Fig. 1. The DAI 1335 was used across

the entire central panel. At each station on the intermediate tapered panel, an airfoil interpolated from DAI 1335 and DAI 1336 was used. On the outermost tip panel, the airfoils were interpolated from DAI 1336 and DAI 1238. This gave a continuous airfoil shape variation across each panel.

The inviscid design pressure distributions of the three Light Eagle airfoils are shown in Fig. 9. The basic design strategy was to increase the length and aft slope of the transition ramp with decreasing Reynolds numbers. This compensates for the increasing reluctance of the boundary layer to undergo transition at the lower Reynolds numbers, but at the risk of premature separation and transition if the actual airfoil geometry is not accurate enough. The actual pressure distributions chosen were a compromise between bubble losses and the tolerance to the level of surface quality expected from the planned construction methods. The bubble loss from this compromise was greatest in the DAI 1335 airfoil, which was used over most of the wing and thus represented the greatest risk. For this reason, the DAI 1335 was designed with a very mild ramp slope. This gave roughly a **6%** drag penalty compared to an ideal ramp.

The length of the ramp on the airfoils, especially the DAI 1335, was the result of the compromise between drag and structural weight. Although a longer ramp gives smaller bubble losses, it also produces larger structural weights due to more solid foam surface beging required to support the polyester film skin against sagging betweeen the ribs over the critical ramp region. Also, a longer ramp results in larger pitching moments, which increase the weight of the wing spar torsion member.

Structural and manufacturing considerations dictated that only a small amount of bottom loading be used in the three airfoils. Although this resulted in a smaller $C_{L\max}$ values than would otherwise be possible with a heavily loaded bottom surface, it gave an all-laminar bottom surface, a modest C_M, and a reasonable trailing-edge angle and camber. The latter two effects produced significant structural and manufacturing advantages.

The drag polars and transition locations calculated by ISES for the three airfoils are shown in Fig. 10. The "standard" external disturbance parameter value of $\&_{\text{crit}} = 9$ was used in these calculations. The calculated surface pressure distributions for DAI 1335 are shown in Fig. 11. The effect of the separation bubble on the upper surface pressure distributions is clearly visible.

The disturbance parameter $\tilde{n}_{\text{crit}}$ has been correlated to freestream turbulence intensity by Mack,[14] although in principle it can represent any physical effect that influences the background disturbances that undergo instability and lead to transition. To determine the sensitivity of the airfoils on disturbance-inducing factors such as vibration or surface roughness, polars were also calculated for $\tilde{n}_{\text{crit}} = 4$ and $\tilde{n}_{\text{crit}} = 14$, corresponding to higher and lower disturbance levels, respectively. The results for the DAI 1335 airfoil are shown in Fig. 12. In general, the higher disturbance level ($\tilde{n}_{\text{crit}} = 4$) causes earlier transition in separation bubbles and thus decreases drag at low lift coefficients where bubble loss is significant. At high lift coefficients, the bubble losses are smaller, and the effect of the higher disturbance level is to substantially move the transition point forward, causing higher drag and lower $C_{L\max}$ due to early trailing-edge separation. The lower disturbance level ($\tilde{n}_{\text{crit}} = 14$) has just the opposite effects. These calculations are consistent with the observed behavior of typical low-Reynolds-number airfoils.

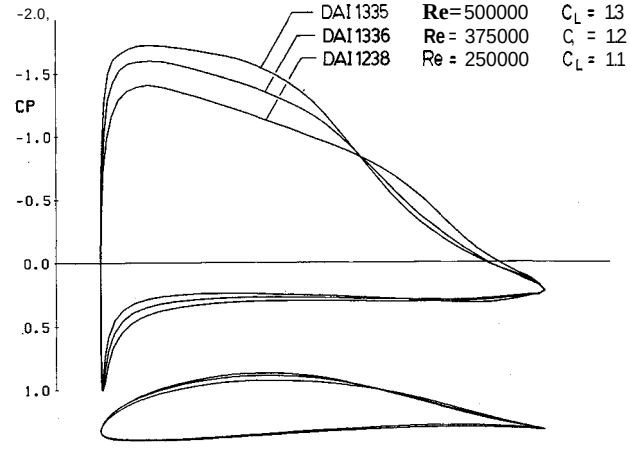

Fig. 9 Design inviscid pressure distributions for the Light Eagle airfoils.

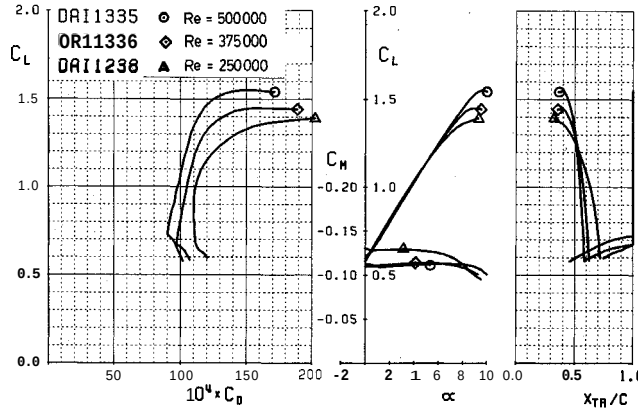

Fig. 10 Calculated operating characteristics of Light Eagle airfoils.

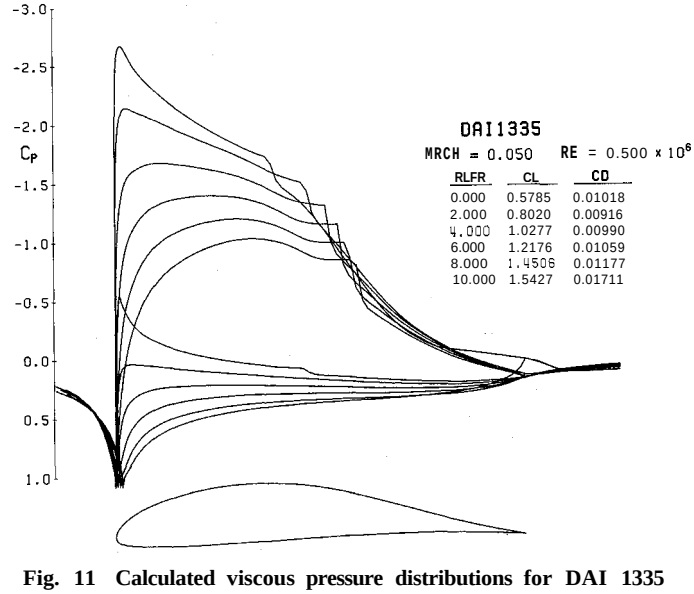

Fig. 11 Calculated viscous pressure distributions for DAI 1335 airfoil.

VIII. Light Eagle Flight Test Results

The Light Eagle airfoils were not tested in a wind tunnel for several reasons. The ISES code had been previously validated in comparison with experimental data,[11,12] and was judged reliable enough to evaluate the airfoil performance, especially for comparison purposes during the design process. Using experimental results to compare airfoil design versions was not possible given the time and cost constraints and would be difficult in the presence of experimental scatter. The absolute performance of the final Light Eagle airfoils was not measured experimentally since it is virtually impossible to duplicate the actual wing surface of the aircraft in a scale wind tunnel model. The actual airfoil contours on the Light Eagle wing deviated visible from the intended shapes due to the 0.0005 in. thick polyester skin sagging or bulging between the

ribs from flight airloads and from the static skin tension. Also, surface roughness has a striking effect on airfoil performance at low Reynolds numbers (as flight tests showed), and the slight graininess of the solid foam sheeting protruding to various degrees through the plastic skin would be impossible to duplicate properly in a scale model. Full-size model testing was ruled out by the lack of a sufficiently large, low-vibration, low-turbulence tunnel. The very-low-disturbance environment present in flight must be closely duplicated in a wind tunnel, since external disturbances have a tremendous effect on low-Reynolds-number airfoil performance.

The flight test data pertaining to airfoil performance consisted of $C_{L\max}$ measurements and flow visualization to determine the transition location across the span. Drag polars of the entire aircraft were also measured via the total energy history (kinetic plus potential) in a glide from a high tow, as described in Bussolari et al.[15] The measured drag was consistent with pilot power as measured via heart rate correlated with ground ergometer data. Unfortunately, extracting profile drag figures from such flight data is riddled with uncertainty, since one must correct for the drag of the fuselage and tail, and for the induced drag in ground effect. Furthermore, there is roughly a 10% scatter present in the measured overall drag figures. **A** more accurate direct drag measurement for an aircraft such as the Light Eagle, which has a sink rate of only 20 cm/s, is nearly impossible. Random vertical air movement of ± 1 cm/s would have produced the 10% scatter observed. Such small vertical velocities are quite undetectable, even in the dead-calm conditions that prevailed during the glide tests.

Since most of the wing surface has the DAI 1335 airfoil or something very similar, the profile drag polar of the overall wing should closely match the DAI 1335 airfoil polar. The highest C_L observed in flight was 1.55, which does indeed correlate well with the DAI 1335 polar shown in Fig. 10. This high value of C_L was obtained by mushing the aircraft in a glide after it was towed to altitude without the propeller.

Flow visualization tests were performed by applying a mixture of kerosene and black powder dye to the wing at various spanwise locations and towing the aircraft at one airspeed for several minutes. The high shear stress of turbulent flow caused the powder dye to flow into a streaked and mottled pattern, while in laminar regions the powder remained in the same smooth, featureless layer as at the time of application. Although the kerosene did not evaporate completely in flight, the powder dye pattern persisted for a sufficiently long time after landing to permit its measurement and photography. Three tests were performed at lift coefficients of 1.04, 1.20, and 1.40. Photographs of the flow patterns on the upper wing surface of the $C_L = 1.04$ test are shown in Fig. 13. The bottom surface of the wing was found to be fully laminar at all operating lift coefficients as expected. Figure 14 shows the top surface spanwise transition lines for the three tests together with the predicted transition lines from the ISES calculations.

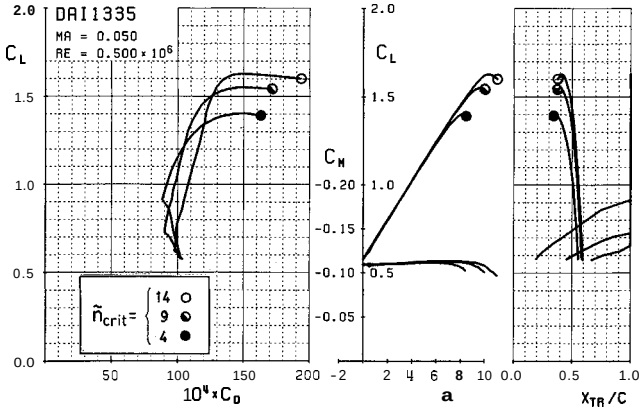

Fig. 12 Calculated DAI 1335 operating characteristics with varying disturbance parameter.

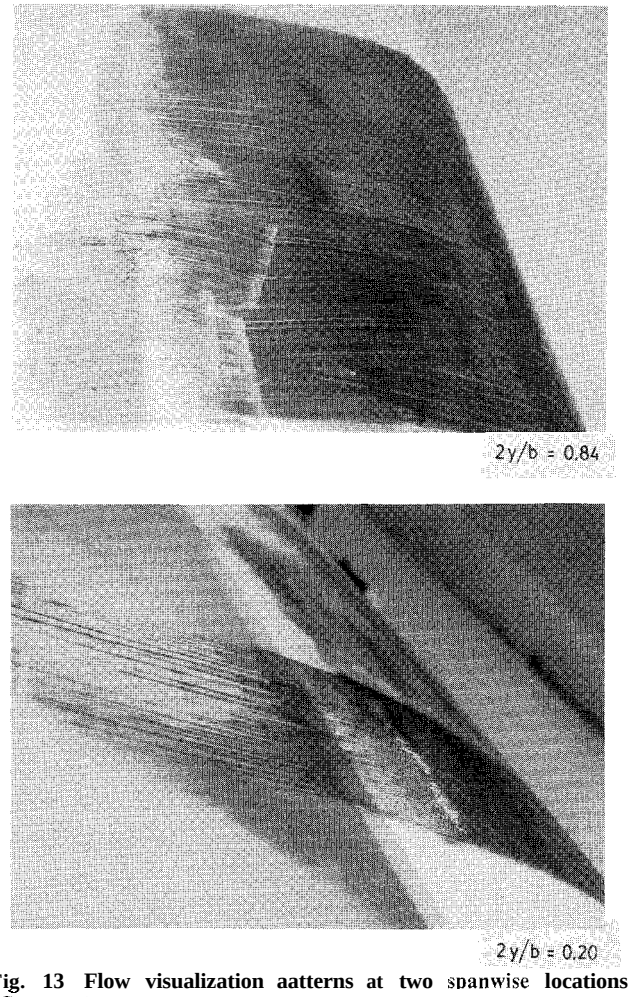

Fig. 13 Flow visualization aatterns at two spanwise locations ($C_L = 1.04$).

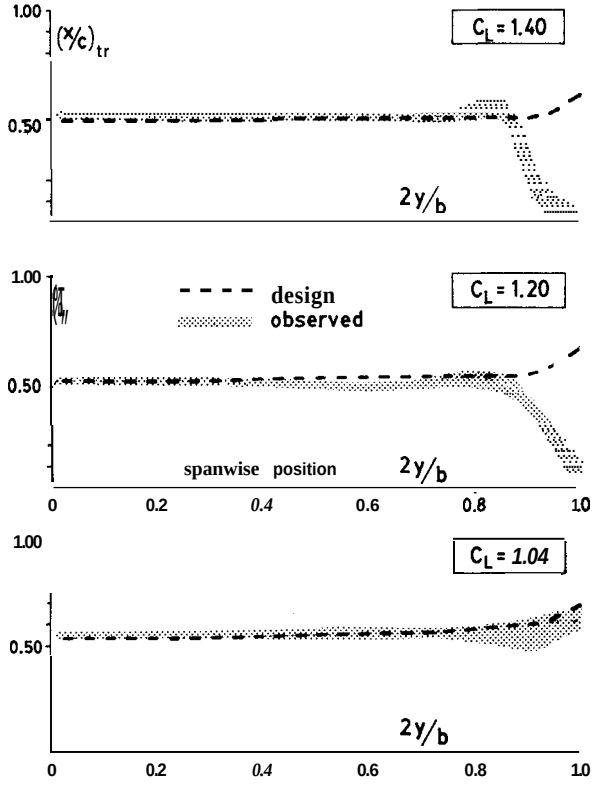

Fig. 14 Transition location results from Light Eagle flow visualization experiments.

The agreement is quite good everywhere except at the wing tip, where premature transition appeared to be occurring. This is attributed to the much rougher surface texture at the leading edge near the tip compared to stations farther inboard. The solid sheeting used to support the plastic skin over the front 65% of the airfoil consists of low-density bead Styrofoam with a rather grainy texture. This rough texture strongly protrudes through the plastic skin at the tip leading edge due to the small leading-edge radius there, thus likely causing the premature transition. Another interesting feature is that near the center of the wing ($2y/b = 0.20$) the transition line is very distinct, indicating that a substantial separation bubble is present. Farther outbord ($2y/b = 0.84$) the changeover from the smooth to mottled pattern is more gradual, implying a weak or even nonexistent bubble, which would naturally produce a "wandering" transition point. This confirms that the DAI 1335 has a stronger bubble than the more aggressive DAI 1336 as intended.

Very early in the flight test program of the Light Eagle, it was found that upper-surface contamination due to frost or dew resulted in a marked aircraft drag increase. This was perceived by the pilots as a substantial increase in flight power. This sensitivity is typical of airfoils with extensive laminar flow regions, such as ones found on sailplanes. The Light Eagle airfoils appear to be no exception. The contamination also had the effect of increasing the minimum-power flight speed. This is consistent with the high-disturbance ISES predictions shown in Fig. 12. With higher disturbance levels, the C_L at maximum L/D is lowered, indicating higher optimum flight speeds.

IX. Conclusions

Three low-Reynolds-number airfoils have been designed via numerical simulation for the Light Eagle human-powered aircraft. A detailed account of the design rationale behind these airfoils has been presented. The central goal of optimizing the overall aircraft performance was strongly driven by minimizing separation bubble losses. Structual and manufacturing constraints were also considered in the airfoil design process.

In-flight flow visualization experiments performed on the Light Eagle showed transition occuring very close to the intended location. Measured $C_{L\max}$ values also closely corresponded to design predictions. The overall performance of the aircraft, measured by glide tests and perceived pilot power output (measured via heat rate), is consistent with the predicted airfoil performance.

Acknowledgment

Support for this work was provided by the Massachusetts Institute of Technology, Office of the Dean of Engineering, and the Smithsonian Institution.

References

[1] Pfenninger, W., "Untersuchen iiber Reibungsverminderungen an Tragfliigeln insbesondere mit Hilfe von Grenzschichtabsaugung," Inst. of Aero. E.T.Z., Ziirich Mitteilung, No. 13, 1946.

[2] Althaus, D., "Influencing Transition on Airfoils," 17th OSTIV Congress, Paderborn, 1981.

[3] Horstmann, K.H. and Quast, A., "Drag Reduction by Means of Pneumatic Turbulators," DFVLR-FB-81-33 Rept. Braunschweig, 1982.

[4] Lighthill, M.J., "On Displacement Thickness," ***Journal of Fluid Mechanics,*** Vol. 4, 1958, pp. 383–392.

[5] Wortmann, F.X., "Airfoil Design for Man Powered Aircraft," Massachusetts Inst. of Technology, Low Speed Symposium, 1974,

[6] Eppler, R., and Somers, D.M., "A Computer Program for the Design and Analysis of Low-Speed Airfoils," NASA TM-80210, Aug. 1980.

[7] Volpe, G. and Melnik, R.E., "The Design of Transonic Airfoils by a Well-Posed Inverse Method," ***Proceedings of the International Conference on Inverse Design Concepts in Engineering Sciences,*** Austin, TX, 1984.

[8] Drela, M., "Two-Dimensional Transonic Aerodynamic Design and Analysis Using the Euler Equations." Gas Turbine Laboratory Rept. 1987, Massachusetts Institute of Technology, Cambridge, MA, Feb. 1986.

[9] Lighthill, M.J., "New Method of Two-Dimensional Aerodynamic Design," Aeronautical Research Council R&M211, June 1945.

[10] Drela, M. and Giles, M.B., "Viscous-Inviscid Analysis of Transonic and Low-Reynolds Number Airfoils," ***AIAA Journal,*** 1987.

[11] Drela, M. and Giles, M.B., "ISES: A Two-Dimensional Viscous Aerodynamic Design and Analysis Code," AIAA Paper 87-0424, Jan. 1987.

[12] Smith, A.M.O. and Gamberoni, N., "Transition, Pressure Gradient, and Stability Theory," Douglas Aircraft Co., Rept. ES 26388, 1956.

[13] Mach, L.M., "Transition and Laminar Instability," Jet Propulsion Lab. Publication 77-15, 1977.

[14] Bussolari, S.R., Langford, J.S, and Youngren, H.H., "Flight Research with the MIT Daedalus Prototype," June 1987.